Ann. Rev. Nucl. Part. Sci. 1987. 37: 33–69

RECENT PROGRESS ON NUCLEAR MAGNETIC DIPOLE EXCITATIONS

Ulrich E. P. Berg[1] *and Ulrich Kneissl*

Institut für Kernphysik, Strahlenzentrum der Justus-Liebig-Universität Giessen, D-6300 Giessen, Federal Republic of Germany

CONTENTS

1. INTRODUCTION AND OUTLINE

Spin vibrations of the atomic nucleus have been studied intensively during recent years with the help of diverse reactions. The study of spin forces, which are based largely on the pion fields of the nucleons, gives us an insight into the magnetic properties of a nucleus. Spin vibrations are observed in charge-exchange reactions, inelastic proton and electron scattering, and nuclear resonance fluorescence experiments. Much new experimental data concerning spin-flip isospin-flip transitions have been obtained during the past decade at modern accelerator laboratories, for example at the Indiana

[1] Present address: Festo Didactic, Ruiter Str. 82, D-7300 Esslingen 1, FRG.

0163–8998/87/1201–0033$02.00

University Cyclotron Facility (IUCF) in Bloomington, Institute de Physique Nucléaire (IPN) in Orsay, the high-resolution electron scattering facility of the Technische Hochschule in Darmstadt, the high-duty-cycle electron accelerator of the University of Illinois in Urbana, and the polarized bremsstrahlung beam of the Universität Giessen.

The giant Gamow-Teller resonance was discovered in (p,n) experiments ten years ago at the Michigan State University cyclotron (1) and has since been systematically studied at IUCF (2–4) with great success. A breakthrough for the investigation of spin-flip transitions with proton scattering was the experiments at very small scattering angles with 200-MeV protons at Orsay (5). These experiments established the existence of the magnetic dipole resonance in heavy nuclei.

Since the nucleon spin is associated with the magnetic moment of the nucleus, it can interact through the electromagnetic field. Therefore, photons and electrons are two interesting probes for studying spin properties of nuclei.

Even before the existence of the giant Gamow-Teller resonance was known, magnetic dipole transitions were being vigorously investigated via inelastic electron scattering, particularly 180° electron scattering. Backward electron scattering is very selective for magnetic multipole excitations. This field of nuclear physics was essentially initiated by Barber and collaborators (6), followed by Fagg and collaborators, who opened up a new line of M1 transition studies (7). Currently the backward-angle inelastic electron scattering experiments with superb energy resolution at Darmstadt and Amsterdam provide much important data for the investigation of spin vibrations in nuclei (8–10).

A new method to probe magnetic dipole excitations with real photons has been developed during the past five years at the University of Giessen linear electron accelerator (11). With the use of linearly polarized bremsstrahlung in nuclear resonance fluorescence experiments it became possible to determine transition probabilities, multipole orders, and parities of dipole transitions to bound states in a completely model-independent manner and with the high accuracy of γ-ray spectroscopy.

Novel observations have been made as a result of studying spin-flip isospin-flip transitions, as discussed below. A completely surprising phenomenon, namely a collective M1 mode, was discovered by Bohle et al (12). A powerful tool to investigate this mode, which does not involve spin-flip transitions but is purely orbital, is the combination of photon (13) and electron scattering data (14).

This review article deals mainly with the investigation of the spin-flip and orbital M1 resonance, with the help of the electromagnetic interaction. Experiments with real photons are emphasized. In the following section the

two different categories of M1 transitions are summarized and connections between different reactions used to study M1 transitions are pointed out. That section is followed by a short description of excitations induced by virtual and real photons at modern electron accelerators. Then the method of investigating M1 excitations with nuclear resonance fluorescence is discussed in some detail and experimental results from that work are presented. Finally first conclusions from the current studies of the collective orbital M1 mode are drawn and new prospects of experiments with real photons are given.

2. CATEGORIES OF M1 EXCITATIONS

The nuclear reactions treated here involve a simultaneous flipping of nucleon spins and isospins. This can be effected in the experiment by the hadronic or the electromagnetic interaction. Theoretical relations between cross sections of such different probes as electrons, nucleons, and pions were recently pointed out by Petrovich et al (15). The Hamilton operator for M1 transitions contains a spin and an orbital part:

$$\tfrac{1}{2}(g_s^p - g_s^n)\vec{\sigma}\vec{\tau} + (g_l^p - g_l^n)\vec{l}\vec{\tau}, \qquad 1.$$

while the Gamow-Teller operator

$$(g_s^p - g_s^n)\vec{\sigma}\vec{\tau} \qquad 2.$$

has no orbital contribution. Spin-flip transitions will be excited by the $\vec{\sigma}\vec{\tau}$ term and orbital excitations by the $\vec{l}\vec{\tau}$ term. In nature, excitations are usually not of pure spin-flip or orbital type but are dominated by one or the other. Under the kinematical conditions of the (p,n) and (p,p′) investigations (2, 16) of the Gamow-Teller and the M1 resonance, respectively, the $V_{\sigma\tau}$ term of the effective nucleon-nucleus interaction is dominant (17).

2.1 *Spin-Flip M1 Excitations*

The relationship between M1, Gamow-Teller (p,n), and β^+ transitions is depicted in Figure 1. This example shows the different 1^+ states, which can be reached via (γ,γ'), (p,p′), (e,e′), (p,n), or (π^+,γ). The initial ground-state spin and parity of ^{26}Mg are $J_0^\pi = 0^+$; its ground-state isospin is $T_0 = 1$ and the third component in isospin space is $T_0^{(3)} = 1$. Absorption of magnetic dipole radiation leads to 1^+ states with isospin $T = 1$ and 2. The strength distribution between the two isospin components, calculated on simple geometrical grounds, is indicated in Figure 1. The M1 resonance is located at about 10 MeV. The analog resonance can be reached by a (p,n) reaction. These states should be located at nearly the same excitation

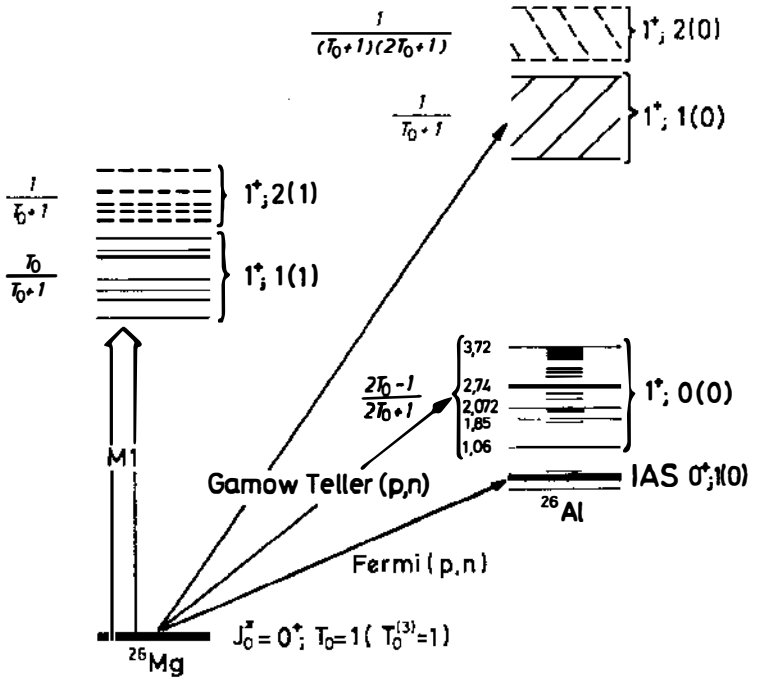

Figure 1 Excitation of spin-flip isospin-flip 1^+ states, differing only in isospin space.

energies above the $J^\pi = 0^+$, $T = 1$ [$T^{(3)} = 0$] isobaric analog state of the ^{26}Mg ground state in ^{26}Al. The two $T = 1$ and 2 excitation regions of 1^+ states in ^{26}Al are shown with cross-hatching in Figure 1. The antianalog states of the M1 resonance in ^{26}Mg, differing only in the isospin quantum numbers [$T = 0$, $T^{(3)} = 0$] are expected to be in the low-energy range of the ^{26}Al level scheme.

If neutron excess is high, as in heavy nuclei, it becomes obvious from the estimate of Gamow-Teller strength distribution among the analog and antianalog states that the antianalog resonance will mainly be populated in a (p,n) experiment. These antianalog 1^+ states of the M1 resonance were the giant Gamow-Teller resonance discovered in (p,n) experiments at the Michigan State University cyclotron (1). Only light nuclei offer the chance to study the analog states of the M1 resonance, and by comparing B(M1) values with (p,n) cross sections, it becomes possible to investigate the orbital part of the M1 transition operator (18–20).

In Figure 2 is shown how the M1 resonance is revealed in a nuclear resonance fluorescence experiment. Peaks due to excitation of 1^+ states

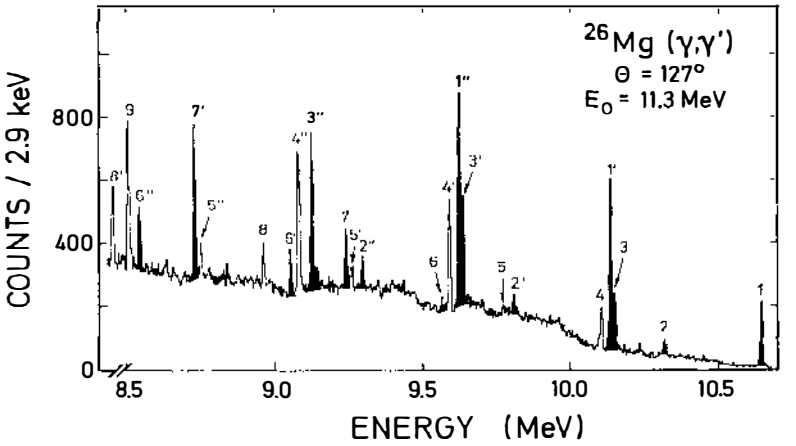

Figure 2 Nuclear resonance fluorescence spectrum from ^{26}Mg. (The peaks are numbered in order.) The solid peaks stem from excitations of 1^+ states. Because of the response of a Ge(Li) γ-ray detector to monoenergetic high-energy γ-rays, single- and double-escape peaks, labeled by one and two primes respectively, occur in addition to full-energy peaks.

are marked. The (γ,γ') spectrum was recorded with bremsstrahlung of 11.3-MeV endpoint energy at a scattering angle of 127°. The parities of the dipole transitions observed were determined with polarized photons, as discussed below.

Roughly the same energy region, but in ^{26}Al as measured in a ^{26}Mg(p,n)^{26}Al experiment, is depicted in Figure 3. Peaks whose angular distributions demonstrate that they belong to excitation of 1^+ states (18) in ^{26}Al are marked too. In addition, B(M1) values from the photon scattering experiment are plotted in Figure 3. The location of 1^+ states in ^{26}Mg and ^{26}Al as well as the distribution of transition strengths are in nice agreement.

2.2 *Orbital Collective M1 Excitations*

Besides the spin-flip excitations discussed in the previous section, a new class of low-lying, collective M1 excitations has been predicted for deformed nuclei in different nuclear models. This collective mode is closely related to the orbital motion of neutrons with respect to protons. The famous electric giant dipole resonance (GDR) (21) represents a familiar example of another kind of an isovector motion. As well known, the main properties of the GDR can be described by hydrodynamical models (22, 23) as an oscillation of neutrons against protons. The mean excitation energies of the GDR are given by

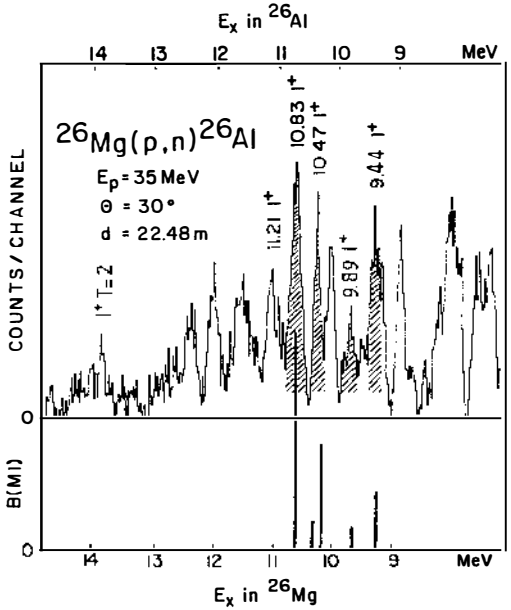

Figure 3 Comparison of M1 transition strengths in ^{26}Mg from nuclear resonance fluorescence (*lower part*) with peaks in a ^{26}Mg(p,n) spectrum due to excitations of the analog 1^+ levels in ^{26}Al.

$$E(\mathrm{GDR}) = 77A^{-1/3}\ (\mathrm{MeV}) \qquad (23) \qquad 3.$$

$$E(\mathrm{GDR}) = 34A^{-1/6}\ (\mathrm{MeV}) \qquad (22) \qquad 4.$$

depending on the choice of the restoring force and the boundary conditions, respectively. For deformed nuclei the GDR splits into two components corresponding to vibrations along the short and long symmetry axes of the deformed nuclei (24).

The macroscopic picture of the hydrodynamical models, describing the GDR, has been adopted by Lo Iudice & Palumbo (25) to construct a collective isovector magnetic mode. In their two-rotor model (TRM) the neutrons and protons are assumed to act as rigid deformed bodies that may rotate against each other around a common axis. An appropriate restoring force leads to a scissor-like oscillation. This geometrical picture of the so-called Scissor Mode makes obvious the predominant orbital character of this excitation. The excitation energy is given in the framework of the TRM by

$$E(\mathrm{M1}) = 42\delta A^{-1/6}\ (\mathrm{MeV}) \qquad (26), \qquad 5.$$

which shows the same A dependence as the GDR resonance energy in the

Goldhaber-Teller model (22). However, the absolute scale is reduced by the deformation parameter δ, which is about 0.25 for strongly deformed nuclei. Therefore, the energy of the M1 mode is lowered to 3–4 MeV whereas the GDR is concentrated at 12–15 MeV in heavy nuclei. This low excitation energy of the M1 mode implies that this mode should be observed in isolated, low-energy, bound states, in contrast to the GDR located in the continuum of highly excited nuclear states.

A large number of theoretical papers have been published on this subject, most of them after the discovery of the new magnetic mode by Richter and coworkers (12). Therefore, this article restricts itself to the rather typical descriptions outlined in the following.

In a sum rule approach (SRA), Lipparini & Stringari (27) showed that the isovector M1 mode can occur by the coupling of a rigid rotation to the isovector giant quadrupole resonance. For the excitation energy, an A dependence has been derived:

$$E(\mathrm{M1}) = 56\delta A^{-1/3} \qquad 6.$$

Microscopic shell-model calculations using the random phase approximation (RPA) also succeeded in describing the new magnetic model to some extent. The excitation energy shows a $\delta A^{-1/3}$ dependence. The scaling factor is about 66 MeV (28). It changes slightly in different calculations, which differ mainly in the choice of the residual interaction. Furthermore, the RPA calculations suggest a fragmentation of the strength into several states (28–31).

Hilton (32) treated the rotational oscillation in his RPA calculation analogously to the linear oscillations of the GDR. In this so-called giant-angle dipole (GAD) model, the excitation energy of the M1 mode is proportional to the GDR energy

$$E(\mathrm{GAD}) = \delta E(\mathrm{GDR}), \qquad 7.$$

in fair agreement with the TRM predictions.

Very recently, parameter-free microscopic calculations of B(M1) strength distributions and decay branchings of the corresponding 1^+ states have been performed by Hammaren et al (33) for some deformed even-even nuclei in the mass region $A = 130$. The total strength of 6–9 μ_0^2 has been predicted to split mainly into two regions at excitation energies of 4 and 5 MeV, respectively.

The interacting boson model can be considered to be between the macroscopic and the shell-model description. In its second version (IBA-2) (34–37), neutron and proton degrees of freedom are treated separately. Neutrons and protons are assumed to couple to pairs (bosons) with angular

momentum $L = 0, 2$, s and d bosons, respectively (in the simplest version). The Hamiltonian, in a simplified form, can be written as

$$H \approx \kappa Q_\nu Q_\pi + \lambda M. \qquad 8.$$

The first term takes into account the quadrupole-quadrupole interaction between neutron and proton bosons and describes the well-known low-lying collective bands in deformed nuclei (see Figure 4). The second so-called Majorana term represents the analogy to the symmetry energy term in hydrodynamical models and determines the separation of states of complete and mixed symmetry with respect to proton and neutron degrees of freedom. The Majorana force parameter λ has to be determined experimentally (see Section 5.3). In the framework of the IBA-2, the orbital M1 mode corresponds to the excitation of a 1^+ state of mixed symmetry, which represents the head of a $K = 1$ band (see Figure 4). The geometrical interpretation of this M1 excitation is a small-angle oscillation of the protons against the neutrons *outside* an inert core. This motion of the "nuclear wobble" (38) likewise suggests that the new M1 mode corresponds to an orbital excitation. Furthermore, a lower strength as compared to the TRM prediction seems to be plausible since only nucleons outside the core participate in the collective motion. The transition strength (39) in the SU(3) limit for axially symmetric rotators amounts to

$$\frac{3}{4\pi}\frac{8N_\nu N_\pi}{2(N_\nu+N_\pi)-1}(g_\nu-g_\pi)^2, \qquad 9.$$

(where N_ν, N_π and g_ν, g_π are the neutron and proton boson numbers and g-factors, respectively).

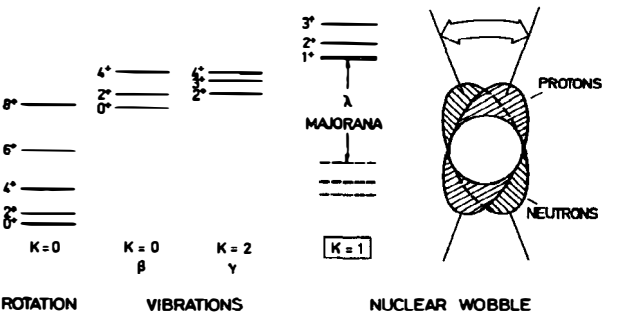

Figure 4 Collective bands of a deformed nucleus and geometrical interpretation of the "nuclear wobble."

In Table 1 the excitation energies and transition strengths as obtained by different model calculations are summarized together with the numerical values for ^{156}Gd, which is the most extensively investigated nucleus so far (14). The theoretical results are compared with the experimental data in Section 5.3.

An extension of the two-rotor model to triaxially deformed nuclei predicts an energetic splitting of the orbital M1 mode (41):

$$\Delta E = E_x \frac{1}{\sqrt{3}} \tan \gamma. \qquad 10.$$

The usual deformation parameter γ describes the deviation from axial symmetry. The strength should be shared within the two states according to

$$B_2(\mathrm{M1})/B_1(\mathrm{M1}) = \left(1 - \frac{1}{\sqrt{3}} \tan \gamma\right) \Big/ \left(1 + \frac{1}{\sqrt{3}} \tan \gamma\right), \qquad 11.$$

which is on the order of unity for small deformation parameters.

In conclusion, the signatures of the new orbital M1 mode in deformed nuclei are

1. an excitation energy of about 3 MeV (in the rare earth region),
2. a transition strength on the order of 3 μ_0^2, and
3. a predominantly orbital character corresponding to convection current type excitations; no or very weak excitation in (p,p′) reactions.

Adequate models must describe the electron scattering form factors as well as the photon scattering data (at the photon point).

3. ELECTROMAGNETIC PROBES

3.1 *Electromagnetic Excitations by Virtual and Real Photons*

The application of elcctromagnetic probes (electrons or photons) in nuclear structure studies offers some fundamental advantages. First of all, the excitation is due to the well-known electromagnetic interaction of the incident electrons or photons with the nuclear charge, current, and magnetization densities. Furthermore, the interaction is weak; therefore, the processes can be treated in perturbation theory, and precise, detailed, and rather model-independent information on the nuclear structure can be extracted. In the following, some basics of electron and photon scattering are summarized that are relevant for understanding the experiments discussed later in this article. For a deeper insight the reader is referred to

Table 1 Model predictions for the excitation energy and $B(M1)\uparrow$ values of the orbital M1 mode

Model	Ref.	Excitation energy (MeV)	Total strength $B(M1)\uparrow$ (μ_0^2)	Numerical values for ^{156}Gd	
				E_x (MeV)	$B(M1)\uparrow$ (μ_0^2)
TRM	(25, 26)	$42\,\delta A^{-1/6}$	$0.035\,\delta A^{3/2}$	4.54	17.12
SRA	(27)	$56\,\delta A^{-1/3}$	$0.043\,\delta A^{4/3}$	2.61	9.06
RPA	(28)	$66\,\delta A^{-1/3}$	$0.027\,\delta A^{4/3}$	3.08	5.69
	(29)		$0.044\,\delta A^{4/3}$		9.27
	(30)		$0.043\,\delta A^{4/3}$	2.5–4.1	9.06
GAD	(32)	δE(GDR)	$0.189\,\delta\,\frac{(N\cdot Z)^{4/3}}{N^{4/3}+Z^{4/3}}\,(g_p-g_n)^2$	3.59	7.53
IBA-2	(39)		$\frac{3}{4\pi}\,\frac{8\cdot N_\pi\cdot N_\nu}{2(N_\pi+N_\nu)-1}\,(g_\pi-g_\nu)^2$		2.91[a]
					3.84[b]

[a] Bare g-factors.
[b] Effective g-factors (40).

the textbooks of Überall (42) or one of the excellent review articles on this subject (43, 44).

Inelastic scattering of an electron on a nucleus can be understood as an exchange of a virtual photon of energy ω and momentum q (see Figure 5). The energy of the virtual photon corresponds to the excitation energy transferred to the nucleus and is determined by the energy loss of the scattered electron. The transfer of momentum q can be varied for a fixed excitation energy by changing the scattering angle and/or the energy of the incident electrons according to

$$\begin{aligned} q &= (k_1^2+k_2^2-2k_1k_2\cos\theta)^{1/2} \\ \omega &= k_1-k_2 \end{aligned} \qquad 12.$$

($k_{1,2}$ are the momenta of the incident and scattered electrons, respectively; in units of $\hbar = c = 1$). This possibility of the q variation in electron scattering enables one to map out the spatial distributions of the change, current, and magnetization transition densities, whereas in experiments with real photons the transfer of momentum is fixed and equal to the excitation energy. Therefore only transition probabilities can be extracted from real photon experiments.

Although electron scattering experiments, in particular on heavy nuclei, have to be analyzed in a Distorted Wave Born Approximation (DWBA), in the following the relevant features of electron scattering are summarized in a Plane Wave Born Approximation (PWBA) description since in this treatment the underlying physical processes are more transparent.

In PWBA the inelastic electron scattering cross section can be written as a sum of cross sections for excitation of different electric and magnetic multipolarities:

$$\frac{d\sigma}{d\Omega} = \sum_{\lambda=0}^{\infty} \frac{d\sigma^{\lambda}}{d\Omega_{cl}} + \sum_{\lambda=1}^{\infty} \frac{d\sigma^{\lambda}}{d\Omega_{magn}} . \qquad 13.$$

The cross section for the excitation of a transition with multipolarity λ

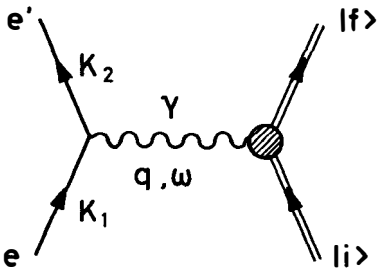

Figure 5 Kinematics of inelastic electron scattering in the one-photon-exchange approximation

can be factorized (neglecting recoil effects) into the Mott cross section, describing the electron scattering on the Coulomb potential of a point-like proton, and a sum of form factors taking into account the spatial extension of the nucleus and being responsible for the diffraction pattern of the scattering cross section:

$$\frac{d\sigma^{\lambda}}{d\Omega} = 4\pi\sigma_{\text{Mott}}\left\{|F_L^{\lambda}(q)|^2 + \left[\frac{1}{2} + \tan^2(\theta/2)\right]\cdot(|F_E^{\lambda}(q)|^2 + |F_M^{\lambda}(q)|^2)\right\}. \qquad 14.$$

The form factors correspond to matrix elements of the multipole operators. The longitudinal (with respect to the q axis) Coulomb form factor F_L is connected to the charge transition density; the transverse electric and magnetic form factors F_E and F_M are related to the convection current and magnetization transition densities. A measurement of the scattering cross section at a fixed q and at different scattering angles allows one to disentangle longitudinal and transverse contributions (Rosenbluth plot; see Equation 14).

For the discussion of low-q electron scattering and its relation to photon scattering it is useful to express the form factors by the corresponding transition probabilities:

$$\begin{aligned} B(C\lambda, q) &= [(2\lambda+1)!!/q^{\lambda}]^2 \cdot |F_L^{\lambda}(q)|^2 \\ B(E\lambda, q) &= [\lambda/(\lambda+1)]\cdot[(2\lambda+1)!!/q^{\lambda}]^2 \cdot |F_E^{\lambda}(q)|^2 \\ B(M\lambda, q) &= [\lambda/(\lambda+1)]\cdot[(2\lambda+1)!!/q^{\lambda}]^2 \cdot |F_M^{\lambda}(q)|^2. \end{aligned} \qquad 15.$$

The scattering cross sections are then

$$\frac{d\sigma^{\lambda}}{d\Omega_{el}} \sim q^{2\lambda}\cdot[V_L(\theta)\cdot B(C\lambda, q) + V_T(\theta)\cdot B(E\lambda, q)]$$

$$\frac{d\sigma^{\lambda}}{d\Omega_{magn}} \sim q^{2\lambda}\cdot[V_T(\theta)\cdot B(M\lambda, q)]. \qquad 16.$$

In the context of magnetic excitations it should be noted that the kinematical function $V_L(\theta)$ vanishes at $\theta = 180°$ whereas V_T (180°) remains finite. Therefore magnetic transitions should be studied at backward angles.

The transition probabilities $B(\lambda, q)$ as measured in (e, e′) experiments depend on the transfer of momentum q; on the other hand, the same transition probabilities at the photon point ($q = \omega$) describe the photoabsorption and the ground-state γ decay of excited levels. The photoabsorption cross section integrated over the level width equals

$$\int \sigma(\omega)\,\mathrm{d}\omega = (2\pi)^3\alpha \sum_{\lambda=1}^{\infty} \frac{(\lambda+1)\omega^{2\lambda-1}}{\lambda[(2\lambda+1)!!]^2}\cdot[B(\mathrm{E}\lambda,\omega)+B(\mathrm{M}\lambda,\omega)] \qquad 17.$$

and the ground-state decay width of an excited level with spin J amounts to

$$\Gamma_0 = 8\pi\alpha \sum_{\lambda=1}^{\infty} \frac{(\lambda+1)\omega^{2\lambda+1}}{\lambda[(2\lambda+1)!!]^2}\,\frac{2J_0+1}{2J+1}\cdot[B(\mathrm{E}\lambda,\omega)+B(\mathrm{M}\lambda,\omega)]. \qquad 18.$$

The transition probabilities $B(\lambda, q)$ as extracted from (e, e′) experiments can be related to the photon scattering data by an extrapolation of the form factors to the photon point. The photon point is not accessible in electron scattering since it corresponds to a scattering angle of 0°. Furthermore the increased background of the radiation tail of the elastic peak makes (e, e′) experiments extremely difficult at forward scattering angles. In addition one deals with rather low cross sections near the photon point since the form factors scale proportionally to q^2. The model-independent PWBA analysis of electron scattering data is limited to experiments on light nuclei and to the use of high electron energies. In a realistic analysis, in particular when dealing with heavy nuclei, the necessary DWBA treatment leads to a certain model dependence of the results. Therefore, the comparison of (e, e′) and (γ, γ') data is of crucial importance in many cases. The information from virtual and real photon work complement one another and supply detailed insights into nuclear structure. As an example of the power of this tool, form factors of the 2.974-MeV 1^+ state in ^{156}Gd (see Section 5.3), predicted by IBA-2 and two-quasi-particle ($2\nu f_{7/2} \rightarrow 2\nu f_{5/2}$) calculations (14, 12), are depicted in Figure 6. The limited,

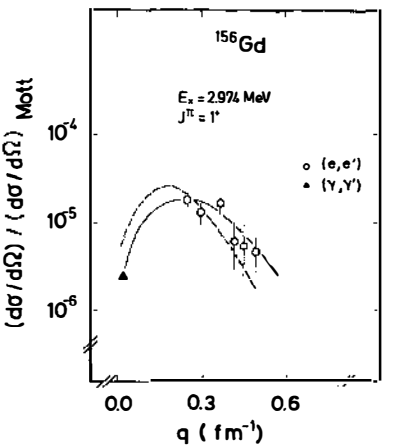

Figure 6 Form factor of the 2.974-MeV state in ^{156}Gd as calculated in IBA-2 (*solid line*) (14) and a two-quasiparticle ($2\nu f_{7/2} \rightarrow 2\nu f_{5/2}$) calculation (*dashed line*) (12) in comparison with (e, e′) and (γ, γ') data (14).

accessible q range makes it impossible to distinguish between the two model calculations on the basis of the (e, e′) data only. However, both calculations differ considerably at the photon point. Therefore, the photon scattering data (13, 14) enable one to reach a clear conclusion as to which model is appropriate.

3.2 *Experimental Progress*

During the past years considerable progress was made in experimental techniques for investigating nuclear magnetic excitations with electromagnetic probes. In present day inelastic electron scattering experiments, measurements can be performed with resolutions comparable to those obtained in hadron-induced reaction studies. An important innovation has been the development of energy loss spectrometer arrangements. By matching the dispersion of the beam transport system to that of the spectrometer, electrons with a certain fixed energy loss were focussed into a single spot of the focal plane, independent of the momentum uncertainty of the incoming beam. Typical relative energy resolutions dE/E of some 10^{-4} can be achieved at modern electron spectrometers working in the energy loss mode. Furthermore, these installations make available beam intensities higher than conventional spectrometer arrangements because a rather broad momentum interval can be used.

An example of this technique's success is the energy loss arrangement at the 70-MeV Darmstadt electron accelerator (DALINAC) (45), where systematic studies of magnetic excitations have been performed by low-energy, but high-resolution inelastic electron scattering experiments (8, 9). The excellent experimental performance of this facility made possible, for example, the recent discovery of low-lying collective M1 excitations (2–3 MeV) in heavy deformed nuclei (12) (see Section 5.3).

In photon scattering work essential experimental developments can be stated too. The availability of modern electron accelerators led to an intensified use of bremsstrahlung photon beams in nuclear resonance fluorescence (NRF) experiments. This technique has the advantage that all states with considerable ground-state widths can be excited simultaneously as a result of the continuous energy spectrum of bremsstrahlung. There are no limitations as in experiments using monenergetic photons from (n, γ) capture reactions, where a random overlap of the incident γ-ray energy and the energy of the state to be excited is necessary (46, 47). Since the pioneering work in photon scattering of bremsstrahlung on low-lying nuclear states carried out by Metzger (48), high-current electron linear accelerators (linacs) in a wide energy range are in operation; furthermore high-resolution γ-ray spectrometers of good efficiency are now available [large volume Ge(Li) or Ge(HP) detectors].

The high beam intensities of present electron accelerators make it possible for the first time to use off-axis bremsstrahlung with reasonable intensity as a source of linearly polarized photons for nuclear fluorescence experiments. Figure 7 shows the setup of the bremsstrahlung facility as installed at the Giessen linac (11, 49). The electron beam from the accelerator (mean currents up to 300 μA) is bent, its energy analyzed by a magnet system, and then focused on a bremsstrahlung radiator target. A 1 mm thick water-cooled tungsten target is used for the production of an intense unpolarized photon beam (about 10^9 photons/s · MeV). Behind the bremsstrahlung target a dumping magnet cleans the photon beam from electrons. A sophisticated system of collimators and beam hardeners within a 3-m concrete wall delivers a well-collimated photon beam in the experimental area. Two sets of steering coils in front of the radiator target make it possible to change the angle of incidence of the electron beam on the target in order to produce linearly polarized off-axis bremsstrahlung. In this operation mode thin aluminum foils (12–50 μm) are used as a radiator. In the experimental area four germanium γ-ray detectors are installed. The degree of polarization can be measured online by a polarimeter based on the photodisintegration of the deuteron (see Section 4.2). The good collimation of the beam, the excellent shielding of the detectors (which reduces the background level), and the high beam intensity enabled systematic NRF studies at the Giessen facility (11, 50) even on enriched isotopes available only in quantities of a few grams.

Conventional electron linacs such as the Giessen machine suffer from

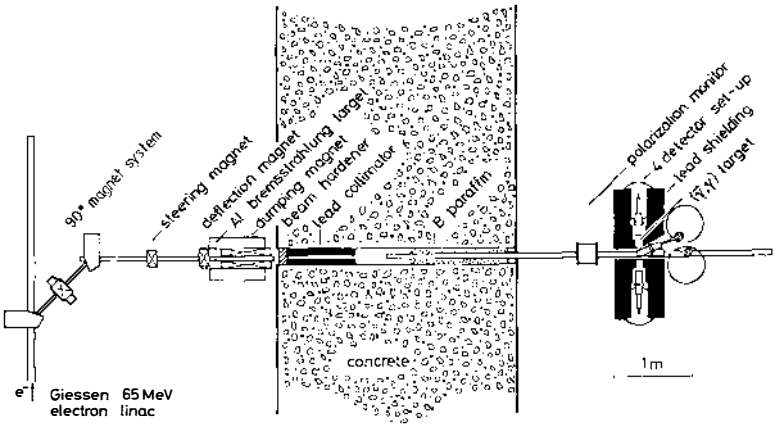

Figure 7 Polarized bremsstrahlung facility for nuclear resonance fluorescence experiments as installed at the 65-MeV Giessen electron linear accelerator (11).

their low duty cycle (on the order of 0.1%). Typical repetition rates are a few hundred hertz. Hence the possible counting rates of the γ-ray spectrometers are limited to less than 10% of the repetition rate in order to avoid pile-up effects. This drawback has been overcome by the construction of the first continuous wave (CW) electron accelerators such as the Microtron Using a Superconducting Linac (MUSL 2) at the University of Illinois (51) and the first stage (14 MeV) of the Mainz Microtron (MAMI) (52). At the continuous beams of such facilities the maximum counting rates in NRF experiments are limited only by the performances of the γ-ray spectrometers and amount to about 5 kHz as compared to about 100 Hz at conventional linacs.

A high duty cycle of the beam also lets one use coincidence techniques, e.g. an efficient production of monochromatic "tagged photons" (bremsstrahlung monochromator) (53). The use of monochromatic photons is a big advantage for the investigation of highly excited continuum states by photon scattering (54). Photon intensities of some $10^5\gamma$/s (in an energy bin of 50–100 keV) could be used in photon scattering experiments (55) at the tagged photon facility of the University of Illinois. Because of their low intensity, the scattered photons were detected by large-volume NaI/Tl γ-ray spectrometers in these experiments. The γ-ray energy resolution of the tagging electron spectrometer (50–100 keV), which is not sufficient to resolve individual bound nuclear states at increased level densities. However, interesting information about mean multipole strength distributions can be obtained from photon scattering with monochromatic tagged photons, in particular when using linearly polarized photons with an enhanced degree of polarization (55, 56) (see Section 4.2).

Besides the new CW electron accelerators, based on high-frequency electron linacs and particular recirculation systems, electrostatic accelerators represent very useful, unique machines for low-energy NRF experiments (48). At the Dynamitron accelerator of the University of Stuttgart (57) a continuous electron beam of up to 4 mA at a maximum energy of 4.3 MeV is available. A high-intensity bremsstrahlung facility has been set up by a Giessen/Köln/Stuttgart collaboration (58) and successfully used for the investigation of low-lying collective M1 excitations in heavy deformed nuclei (13, 14, 59).

4. NUCLEAR RESONANCE FLUORESCENCE WITH LINEARLY POLARIZED PHOTONS

Resonant scattering of bremsstrahlung on an atomic nucleus has become an important spectroscopic method to determine spin vibrations and col-

lective M1 modes in nuclei. The measurement of transition probabilities, spins, and parities in an NRF experiment is completely model independent. On the other hand, exciting a nucleus with photons is very selective; mainly dipole transitions will be induced and to a much lesser degree electric quadrupole transitions.

A breakthrough for NRF experiments with bremsstrahlung was the development of the linearly polarized bremsstrahlung beam facility at the University of Giessen 65-MeV electron linear accelerator (11, 49). With this experimental arrangement it was possible for the first time to determine parities of highly excited dipole states close to the particle threshold in an NRF measurement and to study systematically the spin-flip M1 resonance, which is located around 10 MeV.

4.1 *Formalism of Photon Scattering*

If an atomic nucleus is irradiated by a continuous photon spectrum, it can be excited by multipole radiation of order L_1 or $L_{1'}$ with an energy corresponding to the excitation energy of an excited state. This process and the quantities that influence the photon scattering cross section are shown in Figure 8. The probability of being excited depends on the ground-state transition width Γ_0. The excited level then decays back to the ground state of the nucleus or to a low-lying excited state. The multipole order of the radiation in the exit channel is L_2 or $L_{2'}$ (see Figure 8). The photon scattering intensity for scattering on a nuclear state is directly proportional to the ground-state decay width Γ_0 of a level and the branching ratio to the ground state Γ_0/Γ, where Γ is the total decay width of a state including the decay widths to excited states Γ_f and the particle decay widths, if the level is above particle threshold. The dependence of the photon scattering cross section, integrated over a single resonance, on the decay widths is

$$\frac{d\sigma(\tilde{\gamma},\gamma')}{d\Omega} = \frac{2J+1}{2J_0+1}(\pi\lambda\!\!\!^{-})^2\Gamma_0\frac{\Gamma_f}{\Gamma}\frac{W(\theta,\phi)}{4\pi}, \qquad 19.$$

where $\lambda\!\!\!^{-}$ is the reduced wavelength of the absorbed photon.

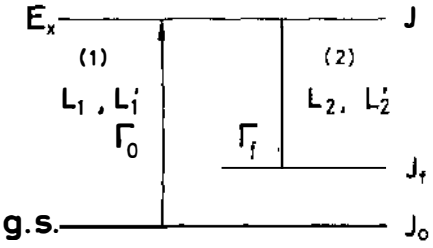

Figure 8 Definition of multipole orders L, decay widths Γ, and spins J; (1) and (2) denote entrance and exit channels.

If thin photon scattering targets are used, self-absorption within the target becomes negligible and the ground-state decay widths Γ_0 can be calculated directly from the photon scattering intensities by using Equation 19. An example of an NRF spectrum obtained in a photon scattering experiment on ^{26}Mg was shown in Figure 2.

The multipole order of a γ-ray transition can be determined by measuring the angular intensity distribution $W(\theta, \phi)$ of the scattered photons. In a (γ, γ') experiment, the axis of quantization is the direction of the well-collimated bremsstrahlung beam. The scattering θ angle is measured between bremsstrahlung beam and emitted deexcitation γ ray; ϕ is the angle between scattering and polarization plane defined by the electrical field vector and the beam direction. The angles relevant for photon scattering are shown in Figure 9.

The angular distributions for dipole and quadrupole radiation from a nucleus with ground-state spin zero are plotted in Figure 10. It is sufficient in this case to measure the intensities of scattered photons at two angles (e.g. at 90° and 127°) in order to determine the multipolarity of a γ-ray transition.

If the bremsstrahlung beam is linearly polarized, an azimuthal asymmetry of the scattered photons will be observed, which in turn can be used to determine the parity of an excitation. The angular distribution for scattering of linearly polarized photons will be

$$W(\theta, \phi) = W(\theta) + (\pm)_{L'_1} \frac{\cos 2\phi}{(1+\delta_1^2)(1+\delta_2^2)} \sum_\nu K_\nu(1) A_\nu(2) P_\nu^{(2)}(\cos\theta), \qquad 20.$$

where $(\pm)_{L'_1}$ equals $+1$ and -1 for electric and magnetic transitions, respectively. $W(\theta)$ is the angular distribution function for scattering of unpolarized photons. Mixing of the radiations of different multipole orders in the entrance channel (1) and the exit channel (2) is determined by the mixing ratio δ. Numerical values for the angular correlation coefficients

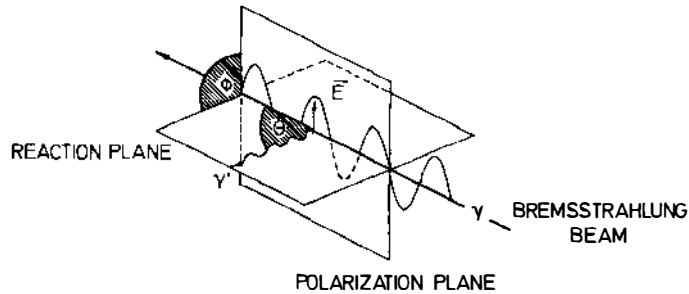

Figure 9 Definition of photon scattering angle θ and azimuthal angle ϕ being relevant in NRF experiments with linearly polarized bremsstrahlung.

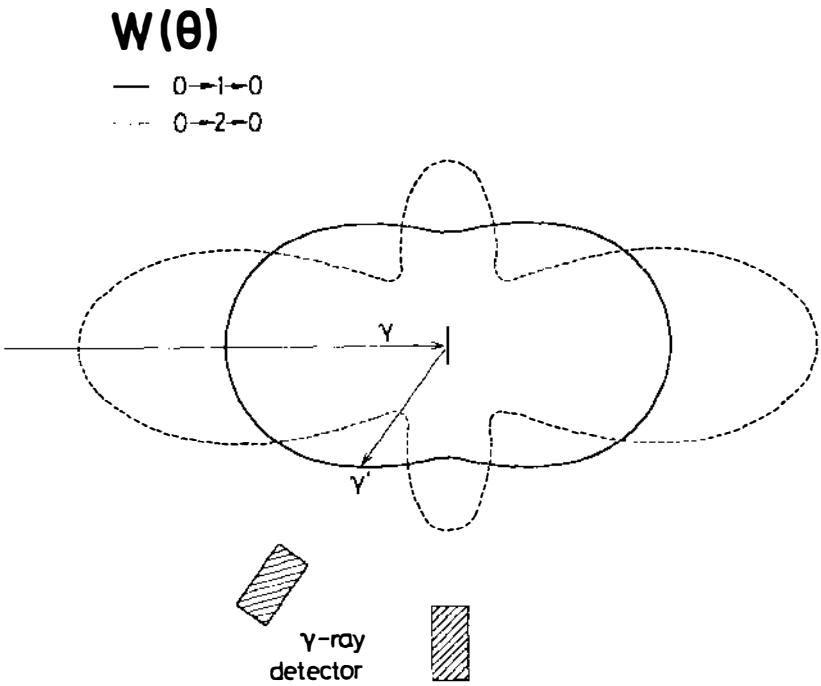

Figure 10 Angular distribution for pure dipole and quadrupole scattering on a ground-state spin $J_0 = 0$ nucleus.

$A_\nu(1)$, $A_\nu(2)$, and $K_\nu(1)$ as well as for the unnormalized associated Legendre functions $P_\nu^{(2)}$ (cos θ) can be found in the review article by Fagg & Hanna (60), "Polarization Measurements on Nuclear Gamma Rays."

Usually, the polarization of the bremsstrahlung beam is $< 100\%$. Therefore, the terms with cos 2ϕ in Equation 20 have to be multiplied by the degree of photon polarization. Figure 11 shows the azimuthal elastic photon scattering intensities at $\theta = 90°$ for pure E1 and M1 excitations of a nucleus with ground-state $J = 0$. Polarization of the incoming photons is assumed to be 100%. In addition, the locations at which the γ-ray dctectors are placed to measure scattering asymmetries are shown.

It is evident from Figure 11 that the number of photons scattered within the polarization plane $N_\parallel$ differ from the number of photons scattered perpendicular to it, $N_\perp$. The measured asymmetry

$$\varepsilon = \frac{N_\perp - N_\parallel}{N_\perp + N_\parallel} = P_\gamma \cdot \Sigma(\theta) \qquad 21.$$

depends o n the degree of bremsstrahlung polarization P_γ and the analyzing

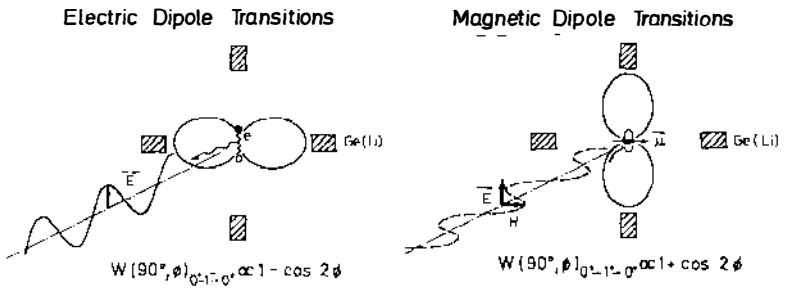

Figure 11 Azimuthal angular distribution of photon scattering cross sections for nuclear resonance fluorescence experiments (electric and magnetic dipole excitations). In both illustrations the direction of the electric field vector E of the incoming γ-ray beam was assumed to be the same. The radiation pattern of oscillating charges e is perpendicular to the photon intensity distribution emitted by a magnetic dipole.

power $\Sigma(\theta)$ of the $(\vec{\gamma}, \gamma')$ reaction. Since the absolute value of $\Sigma(\theta = 90°)$ equals 1 for a spin 0-1-0 cascade, the magnitude of the measured asymmetry is determined by the degree of bremsstrahlung polarization $P_\gamma(E_x)$.

For electric dipole transitions, one will measure asymmetries of $1 > \varepsilon > 0$; for magnetic dipole transitions as well as for electric quadrupole transitions, the range will be $0 > \varepsilon > -1$.

These asymmetries, which are shown later in an asymmetry plot obtained from a measurement with polarized bremsstrahlung on ^{206}Pb, are the basis for parity determination.

4.2 *Production of Linearly Polarized Photons*

As mentioned before, an urgent demand exists for sources of linearly polarized photons with a high degree of polarization, with a high spectral intensity (photons/s·eV), and with variable energy. Unfortunately, these requirements for an ideal source of polarized photons cannot be fulfilled by present techniques. Up to now the application of off-axis bremsstrahlung has been the most successful method for NRF experiments (11).

Since the 1950s, it has been known that off-axis electron bremsstrahlung is partially linearly polarized (61, 62). As schematically shown in Figure 12, the electric field vector E of the bremsstrahlung photons is preferentially perpendicular to the emission plane of the photons and is aligned tangentially to a circle around the incident beam direction. The optimal off-axis angle is about mc^2/E_0 (mc^2 = electron rest energy, E_0 = electron bombarding energy). In order to select off-axis angles that correspond to different directions of the plane polarization, the reaction target can be moved around the central beam (54). Another possibility is to change, by steering coils, the angle of incidence of the electron beam on the

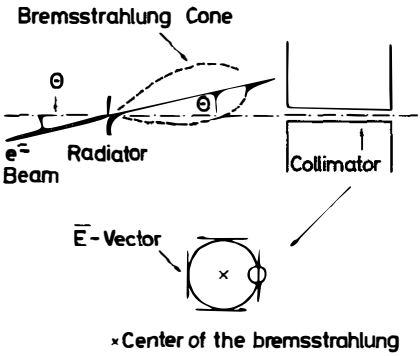

Figure 12 The production of linearly polarized off-axis bremsstrahlung (schematically; see text).

bremsstrahlung radiator target and to select the off-axis angle by a subsequent fixed collimator. The electric field vector then can easily be switched in four directions, as indicated in Figure 12. Furthermore such an arrangement, as installed at the Giessen polarized bremsstrahlung facility (11, 49), offers the advantage of a fixed reaction target position, which allows a fully symmetric setup of four detectors (up, down, left, right). Therefore, all systematic asymmetries of the apparatus can be cancelled in first order.

The degree of polarization can be measured via the photodisintegration of the deuteron. The analyzing power of this fundamental photonuclear reaction has been studied extensively both theoretically (63) and experimentally (64). The analyzing power amounts to nearly unity for moderate energies (< 30 MeV) and emission angles of 90° (63, 64). This means the protons and neutrons are preferentially emitted in the direction of the electric field vector of the polarized bremsstrahlung radiation (for predominant E1 absorption). Because of the two-body disintegration of the deuteron, the energy of the photon inducing the reaction can be determined, even if one is using continuous bremsstrahlung, by measuring the proton or neutron energy. A typical polarimeter consists of four detectors arranged azimuthally around the photon beam. Two types have been realized, based on proton or neutron detection, respectively. When using proton detectors (Si surface barrier detectors or telescopes), the energy dependence of the degree of polarization can be determined more easily (49). However, the neutron detection technique (liquid scintillation counters with pulse shape discrimination) offers the advantage of high counting rates, since thick targets can be used (11).

In Figure 13 a typical dependence of the degree of polarization $P_\gamma(E_\gamma)$ on the photon energy is plotted. P_γ is zero at the bremsstrahlung endpoint energy E_0 (energy of the incident electrons) and amounts to about 30% at

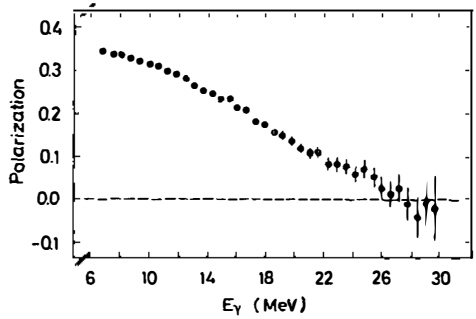

Figure 13 Degree of polarization of off-axis bremsstrahlung as a function of the photon energy ($E_0 = 30$ MeV, $\theta = 1.4°$) (49).

one third of E_0. The photon flux for moderate energies ($E_0 < 30$ MeV) is reduced by a factor of 20 to 30 as compared to that of unpolarized bremsstrahlung beams because of the lower bremsstrahlung yields at off-axis angles and the requirement of a thin radiator target (in order to avoid multiple scattering of the electrons). Therefore, high-current electron accelerators (mean currents of ~ 100 μA) are needed to obtain reasonable polarized photon intensities.

The degree of polarization can be considerably increased by collimation of both the bremsstrahlung quanta and the post-bremsstrahlung electrons. This technique as proposed by Laszweski et al (55) can be applied at tagged photon facilities (bremsstrahlung monochromator). Degrees of polarization on the order of 50% can be achieved at photon energies of about 10 MeV and bombarding energies of 20 MeV. Recently, extensive calculations, in particular of the polarization enhancement, were performed by Ahrens (65) and Sherman et al (66).

The application of polarized off-axis bremsstrahlung in photon scattering work is nicely demonstrated in Figure 14, where results are depicted from a ^{30}Si($\vec{\gamma}, \gamma'$) experiment (50). Four high-resolution Ge(Li) detectors were installed at azimuthal angles of 0, 90, 180, and 270° with respect to the polarization plane defined by the photon beam and the electric field vector. The upper part of Figure 14 shows the pulse height spectra recorded by detectors perpendicular to the polarization plane; in the lower part the corresponding spectrum taken by detectors parallel to the polarization plane is plotted. In ^{30}Si two dipole transitions of 9.357 and 9.792 MeV have been observed in an NRF-experiment using unpolarized bremsstrahlung (67). The corresponding full-energy, single-escape, and double-escape peaks are marked in the spectra as M, M′, M″ and E, E′, E″ respectively. Enhancements of relative intensities are clearly evident: of the "E-peaks"

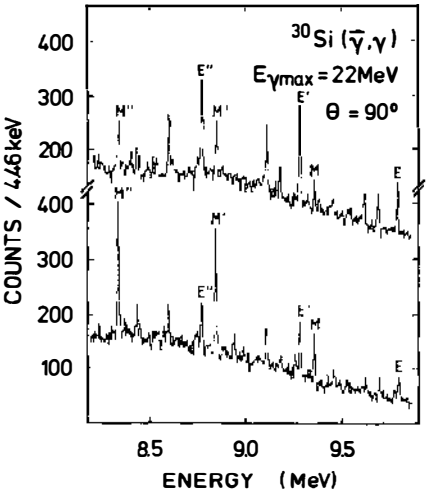

Figure 14 The $(\vec{\gamma},\gamma')$ spectra in an NRF experiment using polarized photons as recorded perpendicular (*upper part*) and parallel (*lower part*) to the polarization plane (see text).

in the upper spectrum and of the "M-peaks" in the lower spectrum. This measured azimuthal asymmetry now allows unique parity assignments (9.357 MeV: magnetic dipole, 1^+; and 9.792 MeV: electric dipole, 1^-). For nuclei with zero ground-state spin, such as ^{30}Si, the analyzing power in a $(\vec{\gamma},\gamma')$ reaction is maximal ($|\Sigma(90°)| = 1$) and changes its sign ($+1$ for electric and -1 for magnetic excitations, respectively). The magnitude of the observed asymmetry then equals the degree of polarization of the photon beam used.

5. RESULTS AND DISCUSSION

Investigation of M1 resonances in nuclei has always been an interesting and challenging puzzle for nuclear physicists. LS closed shell nuclei, such as ^{16}O or ^{40}Ca where no M1 strength was presumed in a single shell model (68), showed considerable spin-flip strength; on the other hand, in jj closed nuclei, such as ^{90}Zr or ^{208}Pb where at least one M1 giant resonance is expected (69), it was difficult to identify the total spin vibration strength (70). Another surprise in the field of nuclear spectroscopy was the discovery of the rotational vibrations of protons against neutrons in deformed nuclei. The status of studies of M1 transitions has been reviewed by Richter (8, 9); here we discuss contributions from the investigation of M1 excitations with polarized and unpolarized bremsstrahlung.

5.1 *Closed Shell Nuclei*

5.1.1 ^{16}O Snover et al (71) found three 1^+ states in ^{16}O with a surprisingly large ground-state M1 strength totalling $B(\mathrm{M1})\uparrow = 0.72\,\mu_0^2$. Some high-

lying M1 strength in addition was found in inelastic electron scattering (72). This M1 strength has been explained by the mixing of core-excited states into the ground state (68) and in second-order perturbation theory (73).

The 16.2-MeV 1^+ state in ^{16}O could also be observed in an experiment with polarized bremsstrahlung (49), and it was shown that the $(\vec{\gamma}, \text{particle})$ reaction provides new information about decay amplitudes of overlapping unbound states of different parity and/or different multipolarity, information not obtainable from unpolarized measurements. The measured $^{16}O(\gamma, p)$ spectrum is depicted in Figure 15 together with the observed analyzing power of this reaction using polarized photons. A clear deviation at 16.2 MeV of the measured from a calculated analyzing power, assuming pure E1 absorption, gives direct evidence that a 1^+ state was excited overlapping with a broad E1 resonance. The $^{16}O(\vec{\gamma}, p)$ experiment yielded decay amplitudes of the 16.2-MeV resonance for the proton decay to the ground state of ^{15}N of $|^1P|^2 = 0.28 \pm 0.010$ and $|^3P|^2 = 0.07 \pm 0.13$ for the singlet and triplet amplitudes.

5.1.2 ^{40}Ca An unexpectedly strong isovector M1 transition was observed in the spin-saturated nucleus ^{40}Ca too (75, 76), which was explained by intense ground-state correlations (75) and by second-order perturbation theory (73). This excitation has also been investigated in an NRF experiment with unpolarized bremsstrahlung (77). The reduced transition probability of the 10.318-MeV level $[B(M1)\uparrow = 1.30 \pm 0.19\ \mu_0^2]$ as obtained in the photon scattering experiment agrees within the error bars with the

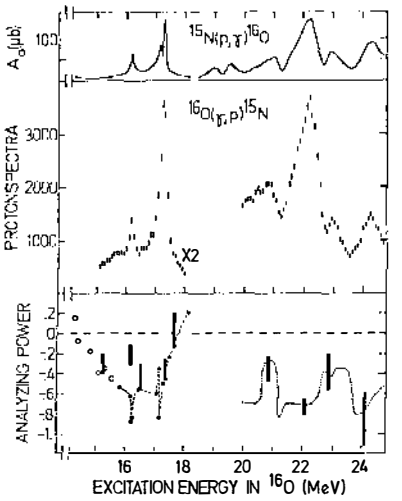

Figure 15 Nuclear photoeffect with polarized bremsstrahlung. The upper panel shows the cross section from the inverse reaction (74). The middle part gives the measured $^{16}O(\gamma, p)$ cross section. In the lower part the observed analyzing power at 90° is presented as error bars together with calculated values taking a_2 coefficients from literature and assuming pure E1 absorption. The data are as follows: open circles from (74); solid circles and dashed line from (71); and dotted line from (71a).

results of the inelastic electron scattering experiment (75) ($1.12 \pm 0.07\ \mu_0^2$), but in addition to the ground-state decay width, the partial decay widths to other states could be measured in NRF (77).

5.1.3 ^{90}Zr Inelastic scattering of 200-MeV protons reveals a pronounced bump at an excitation energy between 8 and 10 MeV (16); this bump has been assigned to the spin vibration mode in this nucleus. More recent ^{90}Zr(p, p′) measurements with polarized protons were able to resolve fine structure in the M1 resonance bump and to settle the spin-flip character of that excitation (78).

High-resolution NRF experiments with unpolarized photons revealed that a bump observed at 9 MeV in a photon scattering measurement with tagged photons consisted of a large number of individual transitions (11). First results from a measurement with polarized bremsstrahlung, however, showed that none of the strongest dipole transitions observed in NRF are due to an M1 excitation (11). In this case the M1 excitation region is covered by very strong E1 transitions. On the other hand, the measurements with polarized photons show that the M1 resonance must be strongly fragmented between many states, because the strong transitions, for which parities could be determined, were E1 excitations. Here measurements with tagged polarized photons, which are currently carried out at Urbana, can help to determine total M1 and E1 strengths (56, 79).

5.1.4 ^{206}Pb AND ^{208}Pb The NRF experiments with polarized bremsstrahlung led to the discovery of the isoscalar M1 transition in ^{208}Pb (80). The isoscalar character of this state, which has also been excited in a ^{209}Bi(d, ^{3}He) reaction (81), was established later by inelastic electron electron and proton scattering experiments (82, 83). This M1 transition is explained in a two-state model as a destructive interference of neutron and proton spin-flip excitations:

$$|1^+\rangle = \alpha|\pi h_{11/2}^{-1} h_{9/2}\rangle - \beta|\nu i_{13/2}^{-1} i_{11/2}\rangle, \qquad 22.$$

with $\beta < 0$ and $\alpha^2 + \beta^2 = 1$. The discovery of the isoscalar magnetic dipole transition in ^{208}Pb at $E_x = 5846$ keV solved a long-standing problem concerning the isoscalar M1 strength in this nucleus. The present state of knowledge concerning M1 strength in ^{208}Pb has been summarized by Laszewski & Wambach (84). The existence of the isoscalar M1 state in ^{208}Pb prompted the question of whether this $J^\pi = 1^+$ state survives when the two $3p_{1/2}$ neutrons close to the Fermi surface are removed.

Figure 16 shows an asymmetry plot from an NRF experiment with polarized bremsstrahlung on ^{206}Pb (85). Only two states exhibited a negative asymmetry (positive parity): the one at 4116 keV, which was a previously known 2^+ state, and a state at 5800 keV. An angular distribution

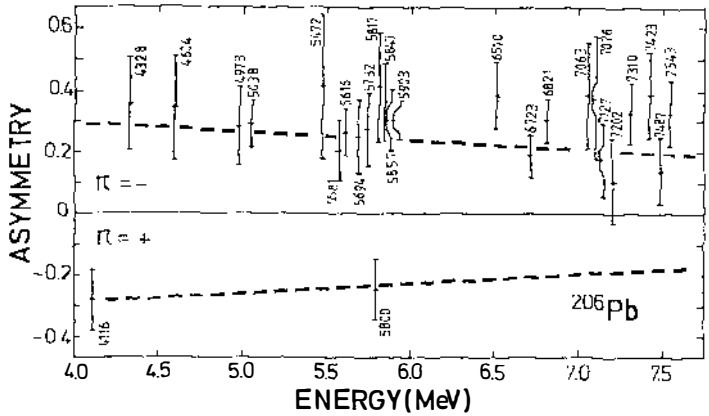

Figure 16 Asymmetries from ^{206}Pb($\vec{\gamma}, \gamma'$) measured with linearly polarized bremsstrahlung (85).

measurement gave evidence that a dipole transition had been detected. It is believed that the 5800-keV transition in ^{206}Pb is an analog transition to the isoscalar M1 transition in ^{208}Pb. A comparison of both M1 transitions in ^{206}Pb and ^{208}Pb from NRF is given in Table 2.

In addition, considerable isovector M1 strength of $19 \pm 2\ \mu_0^2$ between 6.7 and 8 MeV has been detected in ^{206}Pb by Laszewski et al using polarized tagged photons (56).

5.2 *sd-Shell Nuclei*

Two principal mechanisms are considered as likely sources of quenching M1 and Gamow-Teller excitation strength, namely (*a*) "core polarization," or mixing between the valence shell-model space and many highly excited orbits, and (*b*) subnucleonic effects, mesonic exchange currents, and, in particular, Δ-hole excitations (86–88). Quantitative analysis of the degree of quenching must also take into account the effects of configuration mixing within the valence shell-model space.

In the following, a survey of dipole transition strengths to bound states in sd-shell nuclei is given. It was not possible to determine parities of excitations observed in earlier NRF experiments. With the polarized

Table 2 Comparison of the isoscalar M1 states in ^{208}Pb and ^{206}Pb

Isotope	Excitation energy (keV)	B(M1) values (μ_0^2)
^{208}Pb	5846 ± 1	1.6 ± 0.5
^{206}Pb	5800 ± 1	1.5 ± 0.4

bremsstrahlung facility at Giessen, parity determinations became feasible and most of the parities of transitions detected in NRF experiments (50) on even-even nuclei in the sd shell could be determined. In cases where spins were unknown, they were obtained by angular distribution measurements.

The $(\vec{\gamma}, \gamma')$ experiments were performed on ^{22}Ne, ^{26}Mg, ^{28}Si, ^{30}Si, ^{32}S, and ^{34}S. The results of these measurements and a comparison to shell-model calculations are shown in Figure 17. The observed M1 strength in the $T = 0$ isotopes of sd-shell nuclei shows a centroid energy of 11.0 MeV, if the two strong unbound M1 transitions to levels at 11.14 and 11.62 MeV in ^{32}S are included, as reported by Fagg and coworkers (89). Deviations are within 0.5 MeV. It has been pointed out by Kurath (90) that M1 strength should be concentrated in a few levels at the low-energy end of the 1^+ level spectrum.

If two neutrons are added to the $T = 0$ nuclei, the picture changes drastically. A spreading of the M1 strength distribution is observed and strong E1 excitations appear in the realm of the 1^+ states. The B(M1) values of single transitions in $4N+2$ nuclei are, on the average, only 20 and 50% of those in the $4N$ nuclei. The experimental centroid energies of the $T_<$ components of the M1 resonance in $T = 1$ sd-shell nuclei are at 9.2 MeV, with deviations falling within a 1-MeV spread. These results were compared with shell-model calculations, and it was found that the reduction and spreading of M1 strength compared to the extreme jj limit of the shell model could be explained very well by taking into account intra-sd-shell configuration mixing (50). Only about 10% of the configuration mixed shell-model predictions of M1 strengths remain missing, to be accounted for in terms of subnucleonic effects and higher-order core polarization.

5.3 *Deformed Nuclei*

Strong, low-energy M1 excitations have been predicted for heavy, deformed nuclei by several nuclear models, as outlined in Section 2.2. Very recently this new magnetic dipole mode was discovered by Richter and coworkers (12) in rare earth nuclei by high-resolution inelastic electron scattering experiments at the Darmstadt linac. The new mode is of a rather pure orbital character since it could not be excited by inelastic proton scattering (91, 92) where the spin part of the M1 transition operator dominates. Detailed information about the distribution of the orbital, magnetic dipole strength can be extracted from a combined analysis of electron scattering and resonance fluorescence experiments. The reduced transition probabilities obtained by extrapolating the electron scattering form factors to the photon point can be compared with the B(M1)↑ values measured directly at the photon point in photon scattering experiments.

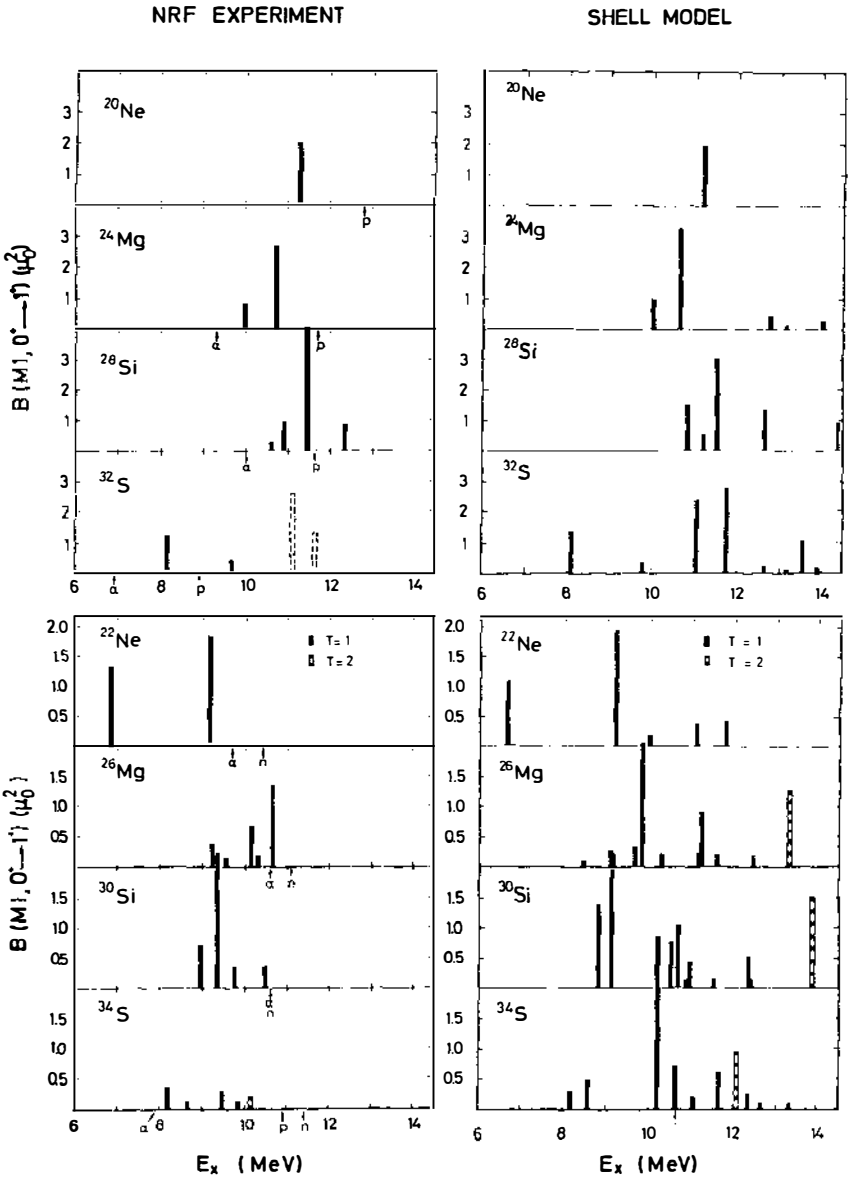

Figure 17 Reduced transition probabilities of bound 1^+ states in $T = 0$ and 1 sd-shell nuclei from nuclear resonance fluorescence measurements performed at the Giessen electron linear accelerator and results from shell model calculations (50). The two B(M1) values plotted as dashed bars were obtained in ^{32}S (e, e′) experiments (89). Particle emission thresholds are indicated by p, n, and α.

As an example, the results for ^{156}Gd are discussed in more detail (14). Figure 18 shows experimental spectra for ^{156}Gd: in the upper part a (γ, γ') spectrum as measured by a Ge(Li) detector at a bremsstrahlung endpoint energy of 3.5 MeV. The marked peaks indicate ground-state transitions. Satellite peaks shifted by 89 keV to lower energies correspond to transitions to the first excited 2^+ states, respectively. The observed branching ratios $R = \Gamma_0/\Gamma_{2+}$ amount to about 2, as is expected for $\Delta K = 1$ transitions within the validity of the Alaga rules (93). The angular distributions of the marked transitions show a clear dipole pattern. In the lower part of Figure 18 the sum of all background-subtracted ^{156}Gd (e, e′) spectra is plotted. Besides the most prominent peak at 3.070 MeV, five weaker magnetic transitions could be detected by the comparison with the (γ, γ') data. The corresponding lines have been cross-hatched in the line decomposition of the (e, e′) spectrum.

In the case of the strong 3.070-MeV transition, the behavior of the electron scattering form factor alone identified the excitation as being due

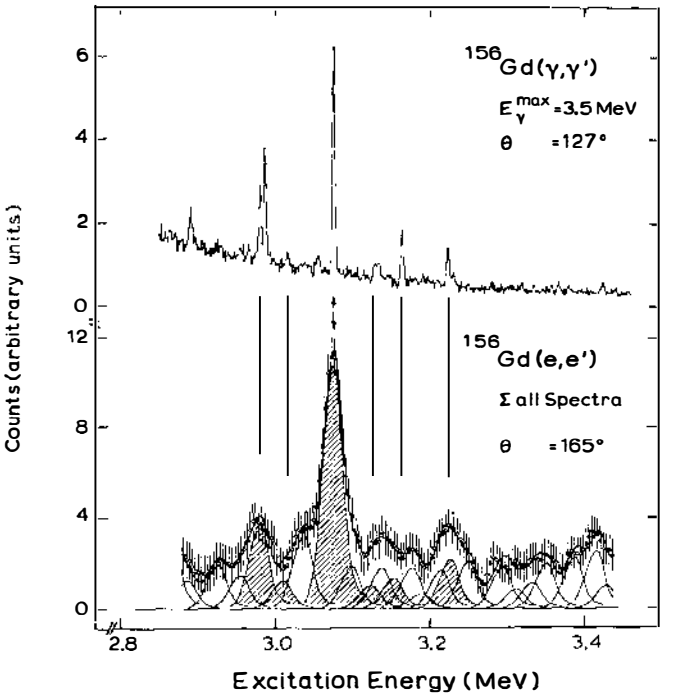

Figure 18 Comparison of nuclear resonance fluorescence and electron scattering spectra in the region of the new M1 mode (14).

to the new mode. However, for the weaker transitions, only a combined analysis of both the (e, e′) and (γ, γ') experiments succeeded in distinguishing between orbital and spin excitations. This is nicely demonstrated in Figure 19, where theoretical M1 transition form factors are compared to the (e, e′) and (γ, γ') data represented by circles and triangles, respectively. The dashed lines show form factors assuming a spin-flip excitation mechanism (12). The full lines correspond to microscopic IBA-2 calculations (14) (orbital excitation). For the weaker transitions, contributions of electric multipoles have been indicated in forward-angle electron scattering data. Therefore, appropriate Tassie model form factors have been added in these cases (14). Figure 19 clearly shows the crucial importance of the photon scattering data enabling an unambiguous distinction between the different form factor calculations. The form factors of all discussed transitions (except the weak 3.158-MeV transition) are well described by the IBA-2 calculations and therefore can be ascribed to the new orbital magnetic mode. Independently, the positive parity of the 3.070-MeV state has been confirmed by a $(\vec{\gamma}, \gamma')$ experiment at the Giessen linac using linearly polarized bremsstrahlung (94).

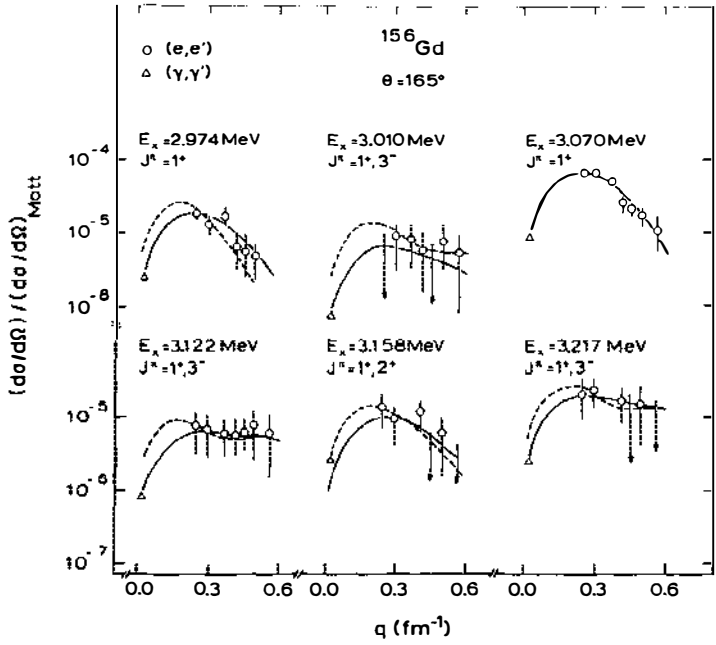

Figure 19 M1 transition form factors in comparison with data from electron scattering and nuclear resonance fluorescence experiments (14). The downward-pointing arrows represent upper limits.

The experimental results of the (γ, γ') and (e, e′) experiments are in good agreement. The observed orbital M1 strength is concentrated in five transitions near 3.1 MeV and amounts to $2.1+0.3\ \mu_0^2$ in the (γ, γ') work compared to $2.3+0.5\ \mu_0^2$ in the (e, e′) experiment. This strength lies below the value of about $3.8\ \mu_0^2$ as predicted by the IBA-2 model in the SU(3) limit (39).

Evidence for the collective magnetic dipole mode in further deformed nuclei in the rare earth region came from systematic (e, e′) experiments performed by the Darmstadt group (95). In the energy range 3.1–3.5 MeV, strong M1 transitions (1–1.5 μ_0^2) of orbital character could be detected in the isotopes ^{154}Sm, ^{158}Gd, ^{164}Dy, ^{168}Er, and ^{174}Yb. In ^{164}Dy a splitting of the strength (about 50 keV) into two main components has been observed and may be connected with a triaxial nuclear deformation (41).

These electron scattering experiments have been complemented by recent NRF experiments of a Giessen/Köln/Stuttgart collaboration. The excellent energy resolution of modern γ-ray spectroscopy (about 3 keV at 3 MeV) and the optimized arrangement at the Stuttgart bremsstrahlung facility (58) led to an increased detection sensitivity of about $0.1\ \mu_0^2$ for M1 transitions in the excitation energy range of about 3 MeV. These experiments are powerful tools for investigating the fine structure and fragmentation of the orbital magnetic dipole strength. Final results have been obtained for the even Gd isotopes (A = 156, 158, 160) and the even Dy isotopes (A = 160, 162, 164) (13, 14, 59, 96). As an example of the observed fragmentation of the strength, the results for the Gd isotopes are plotted in Figure 20. The fragmentation increases with higher mass numbers. The shift of the centroid excitation energy roughly follows the expected 66 $\delta A^{-1/3}$ MeV dependence (28). The total strength, assuming all excitations can be ascribed to the orbital M1 mode, is about 2.4 and 2.7 μ_0^2 for ^{158}Gd and ^{160}Gd, respectively. In the investigated Dy isotopes, the strength is concentrated mainly in two or three states of comparable transition strength (59, 96). The center of excitation energies is shifted from about 2.8 MeV in ^{160}Dy to 3.15 MeV in ^{164}Dy. The total strength observed in this energy range is about 2.5–3.6 μ_0^2.

The new M1 mode is not restricted to the rare earth region. It can also be observed in the other well-known island of deformed nuclei, the actinide region. In spite of the increased experimental difficulties in both electron and photon scattering on these heavy nuclei, a joint Darmstadt/Giessen/Köln/Stuttgart collaboration succeeded in detecting the orbital M1 mode in ^{238}U and ^{232}Th (59, 97, 98). In ^{238}U four prominent transitions near 2.2 MeV could be observed in the (γ, γ') experiments (see Figure 21) whereas in ^{232}Th the strength seems to be mainly concentrated in one transition at 2.043 MeV. The corresponding electron scattering

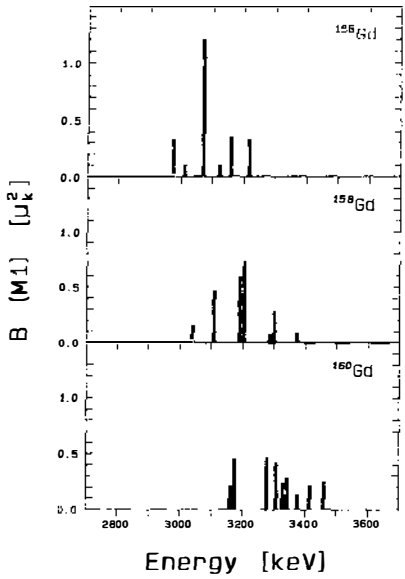

Figure 20 M1 strength distribution in ^{156}Gd and strength distribution of $\Delta K = 1$ dipole transitions in ^{158,160}Gd in the energy range of the orbital M1 mode.

form factors show the M1 character of these excitations. Furthermore, in both isotopes weaker M1 transitions were detected at higher excitation energies: near 2.5 and 2.3 MeV respectively.

Similar collective M1 excitations occur even in light nuclei, as predicted first by Zamick for nuclei in the fp shell (99). The Darmstadt group detected a corresponding 1^+ state in ^{46}Ti at 4.3 MeV (93). In ^{48}Ti, a triaxially deformed nucleus (100) in contrast to the symmetric rotator ^{46}Ti, a pronounced splitting of the M1 strength (3.7 and 5.7 MeV) has been observed (101).

Comparing the experimental results with the theoretical values as summarized in Table 1, it is obvious that the excitation energies can be reproduced well by SRA, GAD, and RPA calculations whereas the TRM prediction overestimates the excitation energy. However, it should be mentioned that a microscopic calculation of the restoring force reduced the excitation energy as calculated in macroscopic models to fairly exactly the experimental values (102).

The experimental excitation energies can be used to adjust the Majorana parameter λ of the IBA-2 Hamiltonian (see Equation 8). The ratio of the Majorana parameter to the deformation parameter δ turned out to be the same for nuclei of different deformations but of the same mass number A. The ratio follows the empirical relation

$$\lambda/\delta = 4.3(N_\nu N_\pi)^{-1/2},$$

where N_ν, N_π are the neutron and proton boson numbers respectively (98).

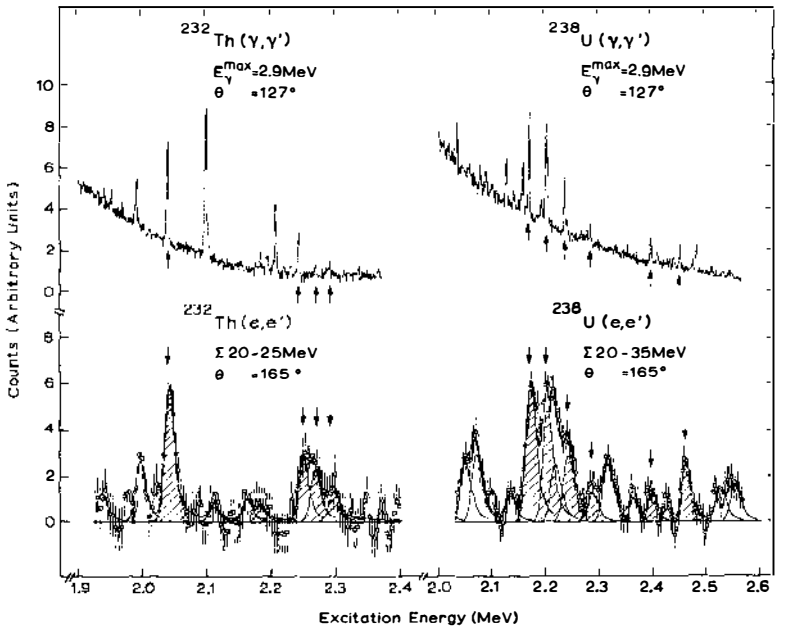

Figure 21 Comparison of NRF and electron scattering spectra for ^{232}Th and ^{238}U (50, 97, 98). The marked peaks correspond to orbital M1 excitations. The strong peaks in the ^{232}Th (γ,γ') spectrum at 2103 keV (^{208}Pb, single-escape peak) and at 2212 keV (^{27}Al) are due to the radioactivity of the target and a calibration reaction, respectively.

The total strength as calculated in macroscopic and RPA models (see Table 1) seems to be too high in comparison to the experimental values. Furthermore, the A dependence given by the RPA calculations (increasing strength proportional to $A^{4/3}$) cannot be confirmed by the experimental findings so far. The IBA-2 results (39) qualitatively agree with the trend of the observed A dependence of the M1 strengths. In particular the predicted strength maximum at $A = 164$ has been confirmed by the (e, e′) data (95). These findings could be corroborated by recent photon scattering experiments (59, 96) in which the highest B(M1) values have been found in ^{164}Dy, too. The absolute values of the M1 strengths observed in the nuclei investigated so far are lower than the model predictions cited in Section 2.3 (TRM, SRA; RPA, GAD, and IBA-2). Closest to the experimental results are the IBA-2 predictions. As an upper limit an exhaustion of 70–90% of the IBA-2 sum rule values (in the rotational limit, bare boson g-factors) can be given for the Gd and Dy isotopes by summing up the strengths of all transitions detected in the high-sensitivity photon scattering experiments in the energy range of interest.

The current knowledge on the orbital M1 dipole mode was reviewed in more detail recently by Richter (97, 101). A survey of the most recent experimental and theoretical progress can be found in the proceedings of the International Conference of Nuclear Structure, Reactions, and Symmetries (Dubrovnik 1986) (103).

6. CONCLUSION AND OUTLOOK

The investigation of M1 excitations is a very lively field in nuclear physics. It was not possible here to cover the whole field completely. Therefore this article focussed mainly on experiments with real photons. Some interesting contributions, both experimental and theoretical, were not discussed: the successful studies of the fp shell with protons (104), electrons (105), and polarized photons; the many approaches to explain the experimentally observed reduction of M1 strength compared to sum rules; or a large number of theoretical articles dealing with the orbital M1 mode.

Some highlights were pointed out, such as the discovery of the isoscalar M1 transitions in Pb nuclei or the discovery of spin vibrations in closed LS-shell nuclei. The importance of ground-state correlations was demonstrated in the systematic investigation of even-even sd-shell nuclei. That nuclear spectroscopy is still exciting was shown by the discovery of a so far unknown phenomenon, namely the orbital rotational oscillations of protons against neutrons in deformed nuclei.

Nuclear resonance fluorescence techniques with linearly polarized photons have progressed considerably. The development of new high-duty-cycle electron accelerators and the construction of new powerful sources of polarized synchrotron radiation (106) give confidence that this method of investigating nuclei has not been exhausted but has a very promising future.

ACKNOWLEDGMENTS

The authors are very grateful to the members of the Giessen photonuclear group for an engaging collaboration during many years: in particular to K. Wienhard, who initiated the Giessen polarized bremsstrahlung facility; to our longtime coworkers K. Ackermann, K. Bangert, C. Bläsing, R. D. Heil, and R. Stock; and to W. Arnold and his linac team. It is a pleasure to thank C. Wesselborg, P. von Brentano (Köln); D. Bohle and A. Richter (Darmstadt), and B. Fischer, H. Hollick, and D. Kollewe (Stuttgart) for a pleasant and stimulating collaboration in the investigations of the new orbital M1 mode. These experiments have been performed at the Stuttgart Dynamitron, where we enjoyed the kind hospitality of the Institut für

Strahlenphysik, under the guidance of Prof. K. W. Hoffmann. A fruitful collaboration with the photonuclear group at Urbana (Illinois) is much appreciated.

The financial support of the Deutsche Forschungsgemeinschaft is gratefully acknowledged.

Literature Cited

1. Doering, R. R., Galonsky, A., Patterson, D. M., Bertsch, G. F. *Phys. Rev. Lett.* 35: 1691–93 (1975)
2. Horen, D. J., Goodman, C. D., Bainum, D. E., Foster, C. C., Goulding, C. A., et al. *Phys. Lett.* 99B: 383–86 (1981)
3. Gaarde, C., Larsen, J. S., Rapaport, J. See Ref. 4, pp. 65–89
4. Petrovitch, F., Brown, G. E., Garvey, G. T., Goodman, C. D., Lindgren, R. A., Love, W. G., eds. *Spin Excitations in Nuclei.* New York: Plenum (1984)
5. Djalali, C. *J. Phys. C* 4: 375–87 (1984)
6. Barber, W. C. *Ann. Rev. Nucl. Sci.* 12: 1–42 (1962)
7. Fagg, L. W. *Rev. Mod. Phys.* 47: 683–711 (1975)
8. Richter, A. *Proc. Int. Conf. on Nucl. Struct.*, Florence, 1983, ed. P. Blasi, R. A. Ricci, pp. 189–217. Bologna: Tipografica Compositori (1983)
9. Richter, A. *Prog. Part. Nucl. Phys.* 13: 1–62 (1985)
10. van der Bijl, L. T., Blok, H., Blok, H. P., Ent, R., Heisenberg, J., et al. *J. Phys. C* 4: 465–69 (1984)
11. Berg, U. E. P. *J. Phys. C* 4: 359–73 (1984)
12. Bohle, D., Richter, A., Steffen, W., Dieperink, A. E. L., Lo Iudice, N., et al. *Phys. Lett.* 137B: 27- 31 (1984)
13. Berg, U. E. P., Bläsing, C., Drexler, J., Heil, R. D., Kneissl, U., et al. *Phys. Lett.* 149B: 59–63 (1984)
14. Bohle, D., Richter, A., Berg, U. E. P., Drexler, J., Heil, R. D., et al. *Nucl. Phys. A* 458: 205–16 (1986)
15. Petrovitch, F., Carr, J. A., McManus, H. *Ann. Rev. Nucl. Part. Sci.* 36: 29–81 (1986)
16. Crawley, G. M., Anantaraman, N., Galonsky, A., Djalali, C., Marty, N., et al. See Ref. 4, pp. 91–109
17. Love, W. G., Franey, M. A. *Phys. Rev. C* 24: 1073–94 (1975)
18. Berg, U. E. P. See Ref. 19, pp. 387–99
19. Goodman, C. D., Austin, S. M., Bloom, S. D., Rapaport, J., Satchler, G. R., eds. *The (p,n) Reaction and the Nucleon-Nucleon Force.* New York: Plenum (1980)
20. Anderson, B. D., McCarthy, R. J., Ahmad, M., Fazely, A., Kalenda, A. M., et al. *Phys. Rev. C* 26: 8–13 (1982)
21. Baldwin, G. C., Klaiber, G. S. *Phys. Rev.* 71: 3–10 (1947)
22. Goldhaber, M., Teller, E. *Phys. Rev.* 74: 1046–49 (1948)
23. Steinwedel, H., Jensen, J. H. D. *Z. Naturforsch.* 5a: 413–70 (1950)
24. Danos, M. *Nucl. Phys.* 5: 23–32 (1958)
25. Lo Iudice, N., Palumbo, F. *Phys. Rev. Lett.* 41: 1532–34 (1978); *Nucl. Phys. A* 236: 193–208 (1979)
26. De Franceschi, G., Palumbo, F., Lo Iudice, N. *Phys. Rev. C* 29: 1496–1509 (1984)
27. Lipparini, E., Stringari, S. *Phys. Lett.* 130B: 139–43 (1983)
28. Bes, D. R., Broglia, R. A. *Phys. Lett.* 137B: 141–44 (1984)
29. Kurasawa, H., Suzuki, T. *Phys. Lett.* 144B: 151–54 (1984)
30. Hamamoto, I., Åberg, S. *Phys. Lett.* 145B: 163–66 (1984); Internal Rep. Lund-MPh 86/07 Univ. Lund (Sweden)
31. Iwasaki, S., Hara, K. *Phys. Lett.* 144B: 9–12 (1984)
32. Hilton, R. R. *Z. Phys. A* 316: 121–22 (1984); *J. Phys. C* 6: 255–64 (1984)
33. Hammaren, E., Schmid, K. W., Faessler, A., Grümmer, F. *Phys. Lett.* 171B: 347–52 (1986)
34. Iachello, F., ed. *Interacting Bosons in Nuclear Physics.* New York: Plenum (1979)
35. Iachello, F. *Nucl. Phys. A* 358: 89c–112c (1981)
36. Dieperink, A. E. L. *Prog. Part. Nucl. Phys.* 9: 121–46 (1983)
37. Dieperink, A. E. L., Wenes, G. *Ann. Rev. Nucl. Part. Sci.* 35: 77–105 (1985)
38. Iachello, F. *Phys. Today* 38: 40–41 (1985)
39. van Isacker, P., Heyde, K., Jolie, J., Waroquier, M., Moreau, J., Scholten, O. *Phys. Lett.* 144B: 1–4 (1984)
40. Sambataro, M., Scholten, O., Dieperink, A. E. L., Piccito, G. *Nucl. Phys. A* 423: 333–49 (1984)

41. Palumbo, F., Richter, A. *Phys. Lett.* 156B: 101–2 (1985); Lo Iudice, N., Lipparini, E., Stringari, S., Palumbo, F., Richter, A. *Phys. Lett.* 161B: 18–20 (1985)
42. Überall, H. *Electron Scattering from Complex Nuclei*, Parts A and B. New York: Academic (1971); *Springer Tracts in Modern Physics* 49: 1–89. Berlin/Heidelberg/New York: Springer (1969)
43. Donnelly, T. W., Walecka, J. D. *Ann. Rev. Nucl. Sci.* 25: 329–405 (1975)
44. Heisenberg, J., Blok, H. P. *Ann. Rev. Nucl. Part. Sci.* 33: 569–609 (1983)
45. Walcher, Th., Frey, R., Gräf, H. D., Spamer, E., Theissen, H. *Nucl. Instrum. Methods* 153: 17–28 (1978)
46. Freund, A., ed. *Proc. Int. Workshop on application of intense capture gamma-ray sources, Nucl. Instrum. Methods*, Vol. 166 (1979)
47. Moreh, R. *Nucl. Instrum. Methods* 163: 275–76 (1979)
48. Metzger, F. R. *Prog. Nucl. Phys.* 7: 54–88 (1959); *Phys. Rev.* 187: 1700–4 (1969)
49. Wienhard, K., Schneider, R. K. M., Ackermann, K., Bangert, K., Berg, U. E. P. *Phys. Rev. C* 14: 1363–66 (1981)
50. Berg, U. E. P., Ackermann, K., Bangert, K., Bläsing, C., Naatz, W., et al. *Phys. Lett.* 140: 191–96 (1984)
51. Axel, P., Cardman, L. S., Hanson, A. O., Harlan, J. R., Hoffswell, R. A., et al. *IEEE Trans.* NS 24(3): 1133–35 (1977)
52. Herminghaus, H., Feder, A., Kaiser, K. H., Manz, W., von der Schmitt, H. *Nucl. Instrum. Methods* 138: 1–12 (1976)
53. O'Connell, J. S., Tipler, P. A., Axel, P. *Phys. Rev.* 126: 228–39 (1962)
54. Nathan, A. M., Starr, R., Laszewski, R. M., Axel, P. *Phys. Rev. Lett.* 42: 221–23 (1979)
55. Laszewski, R. M., Rullhusen, P., Hoblit, S. D., Le Brun, S. F. *Nucl. Instrum. Methods* 228: 334–42 (1985)
56. Laszewski, R. M., Rullhusen, P., Hoblit, S. D., Le Brun, S. F. *Phys. Rev. Lett.* 54: 530–33 (1985)
57. Hammer, J. W., Fischer, B., Hollick, H., Trauvetter, H. P., Kettner, K. U., et al. *Nucl. Instrum. Methods* 161: 189–98 (1979)
58. Heil, R. D. *Proc. Int. Symp. on Symmetries and Nucl. Struct. (SANS)*, Dubrovnik, 5–14 June (1986), ed. R. A. Meyer, F. Iachello, V. Paar, P. von Brentano. Singapore: World Sci. (1986)
59. Kneissl, U. See Ref. 103, 1: 362–67
60. Fagg, L. W., Hanna, S. S. *Rev. Mod. Phys.* 31: 711–58 (1959)
61. May, M., Wick, G. C. *Phys. Rev.* 81: 628–29 (1951)
62. Olsen, H., Maximon, L. C. *Phys. Rev.* 114: 887–904 (1959)
63. Partovi, F. *Ann. Phys.* 27: 79–113 (1964)
64. De Pascale, M. P., Giordani, G., Matone, G., Babusi, D., Bernabei, R., et al. *Phys. Rev. C* 32: 1830–41 (1985)
65. Ahrens, J. Internal rep. Max Planck Inst. Chemie, Mainz. Unpublished (1982)
66. Sherman, N. K., Aniel, T., de Miniac, A. *Natl. Res. Council—Rep. PXNR-2634.* Ottawa, Canada (1982)
67. Ackermann, K. PhD thesis. Giessen (1982)
68. Arima, A., Strottman, D. *Phys. Lett.* 96B: 23–25 (1980)
69. Bohr, A., Mottelson, B. R. *Nuclear Structure*, 2: 636–41. Reading, Mass: Benjamin (1975)
70. Brown, G. E., Raman, S. *Comments Nucl. Part. Phys.* 9: 79–88 (1980)
71. Snover, K. A., Ikossi, P. G., Trainor, T. A. *Phys. Rev. Lett.* 43: 117–20 (1979); Snover, K. A., Adelberger, E. G., Ikossi, P. G., Brown, B. A. *Phys. Rev. C* 27: 1837–65 (1983)
71a. O'Connell, W. J., Hanna, S. S. *Phys. Rev. C* 17: 892–902 (1978)
72. Küchler, G., Richter, A., Spamer, E., Steffen, W., Knüpfer, W. *Nucl. Phys. A* 406: 473–92 (1983)
73. Adachi, S., Lipparini, E., van Giai, N. *Nucl. Phys. A* 438: 1–14 (1985)
74. Earle, E. D., Tanner, N. W. *Nucl. Phys. A* 95: 241–70 (1979)
75. Gross, W., Meuer, D., Richter, A., Spamer, E., Titze, O., Knüpfer, W. *Phys. Lett.* 84B: 296–300 (1979); Steffen, W., Graf, H. D., Gross, W., Meuer, D., Richter, A., et al. *Phys. Lett.* 95B: 23–26 (1980); Steffen, W. PhD thesis. Technische Hochschule, Darmstadt (1984)
76. Crawley, G. M., Anantaraman, N., Djalali, C., Galonsky, A., Jourdain, J. C., et al. *Phys. Rev. C* 26: 87–90 (1982)
77. Moreh, R., Sandefur, W. M., Sellyey, W. C., Sutton, D. C., Vodhanel, R. *Phys. Rev. C* 25: 1824–29 (1982)
78. Nanda, S. K., Glasshausser, C., Jones, K. W., McGill, J. A., Carey, T. A., et al. *Phys. Rev. Lett.* 51: 1526–29 (1983)
79. Laszewski, R. M., Rullhusen, P., Hoblit, S. D., Le Brun, S. F. *Phys. Rev. C* 34: 2013–15 (1986)
80. Wienhard, K., Ackermann, K., Bangert, K., Berg, U. E. P., Bläsing, C., et al. *Phys. Rev. Lett.* 49: 18–21 (1982)
81. Hayakawa, S. I., Fujiwara, M., Imanishi, S., Fujita, Y., Katayama, I., et al. *Phys. Rev. Lett.* 49: 1624–27 (1982)

82. Müller, S., Richter, A., Spamer, E., Knüpfer, W., Metsch, B. C. *Phys. Lett.* 120B: 305–8 (1983); Müller, S., Küchler, G., Richter, A., Blok, H. P., Blok, H., et al. *Phys. Rev. Lett.* 54: 293–96 (1985)
83. Fujiwara, M., Fujita, Y., Katayama, I., Morinobu, S., Yamazaki, T., et al. *J. Phys. C* 4: 453–57 (1984)
84. Laszewski, R. M., Wambach, J. *Comments Nucl. Part. Phys.* 14: 321–40 (1985)
85. Ratzek, R., Berg, U. E. P., Bläsing, C., Jung, A., Schennach, S., et al. *Phys. Rev. Lett.* 56: 568–71 (1986)
86. Bertsch, G. F. *Nucl. Phys. A* 354: 157c–71c (1981)
87. Knüpfer, W., Dillig, M., Richter, A. *Phys. Lett.* 122B: 7–10 (1983); Knüpfer, W., Müller, W., Metsch, B. C., Richter, A. *Nucl. Phys. A* 457: 292–300 (1986)
88. Lawson, R. D. *Phys. Lett.* 125B: 255–59 (1983)
89. Burt, P. E., Fagg, L. W., Crannell, H., Sober, D. I., Stapor, W., et al. *Phys. Rev. C* 29: 713–21 (1984)
90. Kurath, D. *Phys. Rev.* 130: 1525–29 (1963)
91. Djalali, C., Marty, N., Morlet, N., Willis, A., Jourdain, J. C., et al. *Phys. Lett.* 164B: 269–73 (1985)
92. Wesselborg, C., Schiffer, K., Zell, K. O., von Brentano, P., Bohle, D., et al. *Z. Phys. A* 323: 485–86 (1986)
93. Alaga, G., Alder, K., Bohr, A., Mottelson, B. R. *Dan. Mat. Fys. Medd.* 29: 1–22 (1955)
94. Berg, U. E. P. Habilitation thesis. Giessen. Unpublished (1985)
95. Bohle, D., Küchler, G., Richter, A., Steffen, W. *Phys. Lett.* 148B: 260–64 (1984)
96. Wesselborg, C., Berg, U. E. P., von Brentano, P., Fischer, B., Heil, R. D., et al. *Proc. Int. Nucl. Phys. Conf., Harrogate, UK*, p. 88. Inst. Phys. (1986)
97. Richter, A. In *Nuclear Structure 1985*, ed. R. Broglia, G. B. Hagemann, B. Herskind, pp. 469–88. Amsterdam: Elsevier Sci. (1985)
98. Bohle, D., Guhr, Th., Hartmann, U., Hummel, K. D., Kilgus, G., et al. *Proc. Int. Symp. on Weak and Electromagnetic Interactions in Nuclei, Heidelberg*, July 1–5, 1986, ed. H. V. Klapdor, pp. 311–20. Heidelberg: Springer Verlag (1986)
99. Zamick, L. *Phys. Rev. C* 31: 1955–56 (1985)
100. Rebel, H., Hauser, G., Schweimer, G. W., Nowicki, G., Wiesener, W., Hartmann, D. *Nucl. Phys. A* 218: 13–42 (1974)
101. Richter, A. *Phys. Blätter* 49: 313–21 (1986)
102. Nojarov, R., Bochnacki, Z., Faessler, A. *Z. Phys. A* 324: 289–98 (1986)
103. Meyer, R. A., Paar, V., eds. *Proc. Int. Conf. on Nuclear Structure, Reactions and Symmetries (NSRS)*, Dubrovnik, 5–14 June 1986, Vols. 1, 2. Singapore: World Sci. (1986)
104. Marty, N., Djalali, C., Morlet, M., Willis, A., Jourdain, J. C., et al. *Nucl. Phys. A* 296: 145c–52c (1983); Djalali, C., Marty, N., Morlet, M., Willis, A., Jourdain, J. C., et al. *Nucl. Phys. A* 388: 1–18 (1982)
105. Eulenberg, G., Sober, D. I., Steffen, W., Gräf, H. D., Küchler, G., et al. *Phys. Lett.* 116B: 113–17 (1982); Sober, D. I., Metsch, B. C., Knüpfer, W., Eulenberg, G., Küchler, G., et al. *Phys. Rev. C* 31: 2054–70 (1985)
106. Chrien, R., Hofmann, A., Molinari, A. *Phys. Rep.* 64: 249–389 (1980)